A&A 514, A64 (2010)
DOI: 10.1051/0004-6361/200913425

Astronomy & Astrophysics

Physical and morphological properties of $z \sim 3$ Lyman break galaxies: dependence on Lyα line emission

L. Pentericci[1], A. Grazian[1], C. Scarlata[2], A. Fontana[1], M. Castellano[1], E. Giallongo[1], and E. Vanzella[3]

[1] INAF – Osservatorio Astronomico di Roma, via Frascati 33, 00040 Monte Porzio Catone, Italy
e-mail: penteric@oa-roma.inaf.it
[2] Spitzer Science Center, Pasadena, CA, USA
[3] INAF-Osservatorio Astronomico di Trieste, via G. B. Tiepolo 11, 40131 Trieste, Italy

Received 8 October 2009 / Accepted 10 February 2010

ABSTRACT

Aims. We investigate the physical and morphological properties of Lyman break galaxies (LBGs) at redshift ~2.5 to ~3.5, to determine if and how they depend on the nature and strength of the Lyα emission.
Methods. We selected U-dropout galaxies from the z-detected GOODS-MUSIC catalog by adapting the classical Lyman break criteria on the GOODS filter set. We kept only those galaxies with spectroscopic confirmation, mainly from VIMOS and FORS public observations. Using the full multi-wavelength 14-bands information (U to IRAC), we determined the physical properties of the galaxies through a standard spectral energy distribution fitting procedure with the updated Charlot & Bruzual (2009) templates. We also added other relevant observations of the GOODS field, i.e. the 24 μm observations from Spitzer/MIPS and the 2 MSec Chandra X-ray observations. Finally, using non parametric diagnostics (Gini, Concentration, Asymmetry, M_{20} and ellipticity), we characterized the rest-frame UV morphologies of the galaxies. We then analyzed how these physical and morphological properties correlate with the presence of the Lyα emission line in the optical spectra.
Results. We find that unlike at higher redshift, the dependence of physical properties on the Lyα line is milder: galaxies without Lyα in emission tend to be more massive and dustier than the rest of the sample, but all other parameters, ages, star formation rates (SFR), X-ray emission and UV morphology do not depend strongly on the presence of the Lyα emission. A simple scenario where all LBGs have intrinsically high Lyα emission, but where the dust and neutral hydrogen content (which shapes the final appearance of the Lyα) depend on the mass of the galaxies, is able to reproduce the majority of the observed properties at $z \sim 3$. Some modification might be needed to account for the observed evolution of these properties with cosmic epoch, which is also discussed.

Key words. galaxies: starburst – galaxies: evolution – galaxies: high-redshift – galaxies: fundamental parameters

1. Introduction

A long-debated question concerns the relation between Lyman break galaxies (LBGs), i.e. star-forming galaxies selected by the Lyman break in their spectral energy distribution (e.g. Steidel et al. 1996), and Lyα emitters (LAEs), i.e. star-forming galaxies selected by the strong Lyα emission line through deep narrow-band observations (e.g. Cowie & Hu 1998; Hu et al. 1998; Rhoads & Malhotra 2001). Both techniques have led to the discovery of large numbers of galaxies at increasingly high redshift (e.g. Ouchi et al. 2005; Venemans et al. 2007; Stanway et al. 2007; Ota et al. 2008), with the current record holder a LAE at $z = 6.96$ (Iye et al. 2006). The nature of the high redshift galaxies selected through the Lyα emission line and the link with the star-forming population selected via the Lyman-Break is still unclear (e.g., Gawiser 2009). This relation is crucial for our interpretation of the very high redshift Universe where, due to current instrumental limitations, it becomes progressively easier to spectroscopically confirm only the Lyα emitters (e.g. Dow-Hygelund et al. 2007).

On one hand the Lyα bright phase could represent a stochastic event in the life of any galaxy (as in the duty cycle model of e.g. Nagamine et al. 2008); alternatively it could be related to some specific physical property of the galaxies, like the (young) age, the dust or gas content.

In principle, the Lyα line can be used to probe star-formation rates and clustering properties (Kovac et al. 2007), but also for cosmological applications like re-ionization studies (e.g. Dijkstra et al. 2007; Dayal et al. 2008). In practice, this effort is far from trivial because of the above stated complications. Understanding what determines the Lyα emission line is therefore fundamental to interpret the bias introduced by the observational selection techniques.

A comparison between the physical and morphological properties of LBGs and LAEs is necessary, but not straightforward. Because of the different selection techniques, LAEs tend to be much fainter than LBGs, and therefore modeling their spectral energy distributions (SEDs) to constrain the relevant physical properties has always been a difficult task (see Gawiser 2009, for a review). Most studies rely on stacked photometry and are able to derive only average properties (e.g. Finkelstein et al. 2007; Nilsson et al. 2007; Lai et al. 2008). Furthermore until recently most LAEs samples lacked (deep) data in the mid-IR range, which are crucial to constrain stellar mass at redshift >4, where the 4000 Å break is shifted beyond the K-band. A good coverage of the near-IR was also often missing, and this is important to reduce the model degeneracies (e.g old/dust-free vs. young/dusty

population). Therefore we took a slightly different approach and decided to study the properties of Lyα emitting galaxies selected as LBGs. In this way, we select galaxies that are bright enough in the continuum to be detected at other wavelengths (so their SEDs can be modeled) and show Lyα in emission: we can then study the dependence of physical properties on the emission line strength and characteristics on individual galaxies, rather than relying on the stacking technique. Clearly this is only possible with a survey that has both deep multi-band data on a relatively large area, and excellent spectroscopic coverage. The GOODS survey (e.g., Dickinson et al. 2004; Giavalisco et al. 2004) has all these properties: in particular we took advantage of the excellent observations in the near-IR, which cover the rest-frame region around the 4000 Å Balmer break, reducing some of the model degeneracies. Furthermore, the deep IRAC data allow the determination of stellar masses with great accuracy (e.g. Fontana et al. 2006).

In previous works we compared the properties of LBGs with and without line emission for a relatively small sample of $z \sim 4$ galaxies (Pentericci et al. 2007, hereafter P07) and then studied the properties of a more numerous sample of Lyα emitting LBGs in the redshift range 3 to 6 (Pentericci et al. 2009, hereafter P09). In this paper we study the properties of LBGs at redshift ∼2.5−3.5, the so-called U-dropouts, initially selected from their continuum and color properties and with follow-up spectroscopic confirmation: the lower redshift allows us to assemble a sample much more numerous than in our previous work and study the trends in a statistically more significant way. At the same time, thanks to the brighter average magnitude of the galaxies, we can also attempt a morphological analysis, which was not possible at higher z.

As in previous work, we use the GOODS-MUSIC catalog (Grazian et al. 2006) in its revised and updated version (Santini et al. 2009). In particular the new catalog contains 24 micron data from Spitzer/MIPS observations and a revised and more accurate IRAC photometry. New spectra from public surveys (Vanzella et al. 2009; Popesso et al. 2009) were also added. We additionally include an analysis of the deep X-ray data available for the field, i.e. the 2 Ms Chandra exposure (Luo et al. 2008) which allows us to study the star formation and/or AGN content in an independent way.

All magnitudes are in the AB system (except where otherwise stated), and we adopt the Λ-CDM concordance cosmological model ($H_0 = 70$, $\Omega_M = 0.3$ and $\Omega_\Lambda = 0.7$).

2. The sample

To select $z \sim 3$ galaxies we adapted the usual Lyman break technique to the filters adopted in the GOODS survey, which are different from the classical UGR filter set used by Steidel et al. 2003 (see also Giavalisco et al. 2004). The redshift ∼3 objects are selected as U-dropouts according to the following cuts:

$$-0.2 \leq V - I \leq 0.35$$

$$U - V \geq 0.75(V - I) + 1.15,$$

which are effective at $2.4 \leq z \leq 3.5$. These cuts were determined by Grazian et al. (2007) using our multicolor GOODS-MUSIC database, and from a comparison to the photometric redshift distribution were adjusted to maximize the completeness and minimize the number of interlopers at redshift outside the above range. In that work, we also verified that these criteria are almost (although not entirely) equivalent to the original LBG criteria by reproducing the synthetic UGR magnitudes for the galaxies. However, several differences remain, beside the difference in the filter set and the color selection: first of all the LBGs were traditionally selected in the R-band, which is lacking in the GOODS survey, and not in the z-band, as in this work; furthermore LBGs were originally relatively bright galaxies, since the historical criterion used was $R \leq 25.5$, while in this work the selection is pushed to the nominal completeness of the GOODS-MUSIC sample (z-band magnitude limit of 26.0). All this resulted in some differences in the final sample properties, mainly a redshift distribution of galaxies that was slightly wider than in the Steidel et al. (2003) sample and possibly a slightly bluer average color (see also Sect. 4.1 for this point). Objects flagged as AGNs (on the basis of their X-ray emission, and/or mid-IR excess and/or spectral properties) in the GOODS-MUSIC catalog were not included in the analysis. We found about 450 U-dropouts in the entire GOODS-South. We then cross-correlated this list with the spectroscopic observations available in the area. Spectra of galaxies in the GOODS-South field were obtained by several different observational campaigns: the two most extended ones were conducted by ESO with FORS2 (Vanzella et al. 2006, 2008, 2009) and VIMOS (Popesso et al. 2009). Other redshifts were obtained with the VLT by GMASS (Kurk et al. 2009), by the HST/ACS/G880L grism survey PEARS (Straughn et al. 2008) and the similar GRAPES project (Pirzkal et al. 2004; Malhotra et al. 2005). In total there are 130 U–dropout galaxies with confirmed redshift.

As in P07 we defined as LBG_L the Lyman break galaxies that show the Lyα line in emission, regardless of its strength. We measured the equivalent width (EW) of the Lyα line from the 1D spectra, using the IRAF task splot, by marking two continuum points around the line to be measured. The linear continuum was subtracted and the flux was determined by simply summing over the pixels (no fitting of the line profile was performed). The sample of LBG_L contains 66 galaxies, of which 24 have a rest-frame Lyα equivalent width $EW > 20$ Å and therefore would be selected as LAEs in a narrow band survey. The rest of the LBG_L had a line emission too faint to pass that selection. Lyman break galaxies with no sign of emission or with a clear absorption were called LBG_N and were also 66 (note that two galaxies show both a clear emission line and an absorption and are included in both samples). The two sub-samples were not biased in terms of V-band magnitude or absolute rest-frame luminosity at 1400 Å (see first entry of Table 1). This indicates that for this sample the redshift confirmation of LBGs does not sensibly depend on the presence of emission lines (see also Popesso et al. 2009). In Fig. 1 we plot the redshift distribution of our final sample of galaxies, and for the two sub-samples separately. The overall redshift distribution of our LBGs, and in particular the partial lack of objects around $z \sim 3$, is shaped by the spectroscopic completeness level of the GOODS catalog (plotted in Fig. 6 of Popesso et al. 2009). This spectroscopic catalog is actually formed by a compilation of many different spectroscopic surveys (as discussed earlier), each with its own selection criteria and efficiency: the completeness level is therefore a complicated function of redshift and has a local minimum around $z \sim 3$. For the purpose of the present work, we note that the two sub-samples have a consistent redshift distribution.

3. Spectral energy distribution fitting

The main physical properties of the galaxies like total stellar mass, continuum-based star formation rate, stellar age, dust

Table 1. Average properties of LBG_L and LBG_N derived from the SED-fitting with the Charlot & Bruzual (2009) models.

Property	LBG_L	LBG_N	$P(K-S)$
N_{gal}	66	66	
$L(1400)$ (cgs)	$5.9 \pm 0.6 \times 10^{28}$	$6.0 \pm 0.6 \times 10^{28}$	0.993
SFR_{SED} ($M_\odot$ yr^{-1})	13.2 ± 4.2	16.0 ± 11	0.367
SFR_{UV} ($M_\odot$ yr^{-1})	15.6 ± 1.9	12.9 ± 3.4	0.414
Age (Myr)	250 ± 35	316 ± 40	0.136
$E(B-V)$	0.03 ± 0.009	0.06 ± 0.012	0.012
Mass ($M_\odot$)	$3.4 \pm 1.5 \times 10^9$	$8.7 \pm 1.2 \times 10^9$	0.000

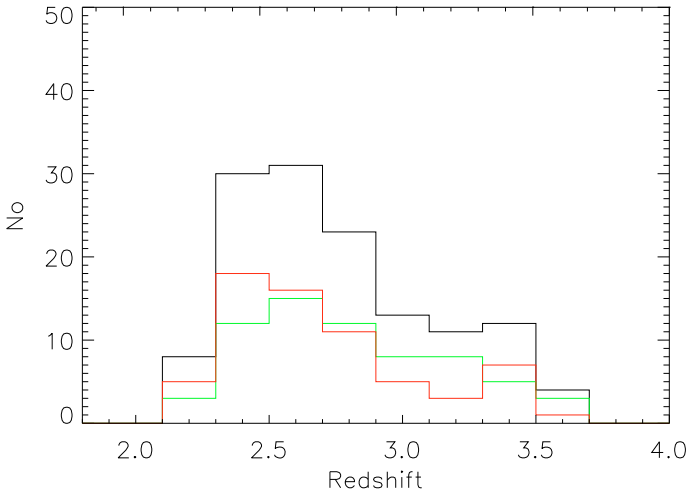

Fig. 1. Distribution of spectroscopic redshifts for the entire sample (black line), the LBG_L sub-sample (green line) and LBG_N sub-sample (red line).

extinction $E(B-V)$ and so on, were obtained through a spectral fitting technique, which was developed in previous papers (Fontana et al. 2003, F06), and is similar to those adopted by other groups in the literature (e.g. Dickinson et al. 2003; Drory et al. 2004). Briefly, a grid of spectral templates is computed from standard spectral synthesis models, and the expected magnitudes in our filter set are calculated. The derived template library is compared with the available photometry, and the best-fit model template is adopted according to a χ^2 minimization. During the fitting process, the redshift is fixed to its spectroscopic value. The physical parameters associated with each galaxy are obtained from the best-fit template up to 5.5 μm rest-frame. This analysis assumes that the overall galaxy SED can be represented as a purely stellar SED, extincted by a single attenuation law and that the relevant $E(B-V)$ and basic stellar parameters (mostly age and star formation history, but also metallicity) can be simultaneously recovered with a multi-wavelength fit. We note that parameter degeneracies cannot be completely removed, especially at high redshift, even if our filter set samples quite evenly the overall wavelength range involved. Previous studies (Shapley et al. 2003, 2001; Papovich et al. 2001) demonstrated that stellar masses are well-constrained, while for other parameters the uncertainties become larger, especially at high redshifts, due to the SFR-age-metallicity degeneracies.

In our analysis, we estimated SFR, AGE Mass, $E(B-V)$ and metallicity using the Charlot & Bruzual (2009 in preparation, hereafter CB09) synthetic models, which fit the whole 14 bands of photometry (namely $U_{3.5}$ and $U_{3.8}$ from the WFI on the ESO 2.2 m telescope, U_{VIMOS}, ACS/HST B, V, i and z, VLT/ISAAC J, H and K, SPITZER/IRAC 3.5, 4.5, 5.8 and 8 μm). Note that the catalog was produced with a specific software for the accurate "PSF-matching" of space- and ground-based images of different resolution and depth, named ConvPhot (De Santis et al. 2007). We assumed a Salpeter IMF and parametrized the star formation histories with a variety of exponentially declining laws (of timescales τranging from 0.1 to 15 Gyr), metallicities (from $Z = 0.02Z_\odot$ to $Z = 2.5Z_\odot$) and dust extinctions ($0 < E(B-V) < 1.1$, using a Calzetti extinction curve). Details are given in Table 1 of Fontana et al. (2004), in Fontana et al. (2006) and in Grazian et al. (2006). The age of each object was constrained to be less than the age of the Universe at the relevant redshift. We also adopted a minimum age of 10 Myr. We are aware that exponential star formation histories may not be the correct choice in some cases, but allowing τ to vary, we can actually reproduce both an instantaneous burst (when τ is very small) and a constant star formation rate (when τ is $\gg$ than the age of the galaxy.)

At variance with our previous work (P07, P09) we use here the new version of the stellar population model described in detail in Charlot & Bruzual (2009). The main improvement over the previous Bruzual & Charlot (2003, BC03) model is an updated treatment of the emission from those stars that are in the thermally-pulsing asymptotic giant branch (TP-AGB) phase of stellar evolution from the models of Marigo & Girardi (2007). As shown first by Maraston (2005, M05) and Maraston et al. (2006), TP-AGB stars are especially important in galaxies whose spectra are dominated by emission from these intermediate age stars.

As already shown by several authors (e.g. Marchesini et al. 2009; Eminian et al. 2008; Lamareille et al. 2008), the CB09 models give masses that are on average lower than the BC03 ones. In particular, the recent study by Salimbeni et al. (2009) on a sample that partially overlaps with the present one showed that the average mass difference in their highest redshift bin (which includes the range $z \sim 2.5-3.5$, see their Fig. 4) is around ~30%, with a slight dependence on mass.

Examples of SED-fitting for some of the galaxies, which span the entire redshift range, are shown in Fig. 2. While [OII] and Hα emission were included in the models with a strength proportional to the SFR according to the Kennicutt (1998) relations, the Lyα and [OIII] emission line were more difficult to model. In particular the Lyα line could contaminate the photometry of the B or V-band (depending on the redshift) and therefore change the result of the SED-fitting. To check this, we performed a second fit, excluding the band that contains the emission line. Alternatively we estimated the Lyα line contribution to the corresponding broad band flux (B-band for $z < 2.9$ and V band for the rest) following Eq. (2) of Papovich et al. (2001) and performed a third fit including the full set of 14 bands. This method is actually somewhat more uncertain, since the EWs were estimated from the 1-dimensional spectra, while the broad band magnitudes were measured from aperture photometry, and we had no information on the relative spatial distribution of the line emitting gas and the stars in each individual object. In any case both fits give results that are entirely consistent with the initial one: this indicates that the Lyα line does not significantly influence the SED-fitting outcome, also because none of the LBG is a strong emitter/absorber. It also confirms the solidity of the fit: the results do not depend on the individual band, thanks to the large number of bands that we used in the fits. Finally we also checked if the [OIII]5007 line contribution could somehow change the results of the SED-fit: the [OIII] line was harder to model, since its strenght is known to vary considerably for a given Hα flux (e.g. Moustakas et al. 2006), and this precludes its suitability as a SF

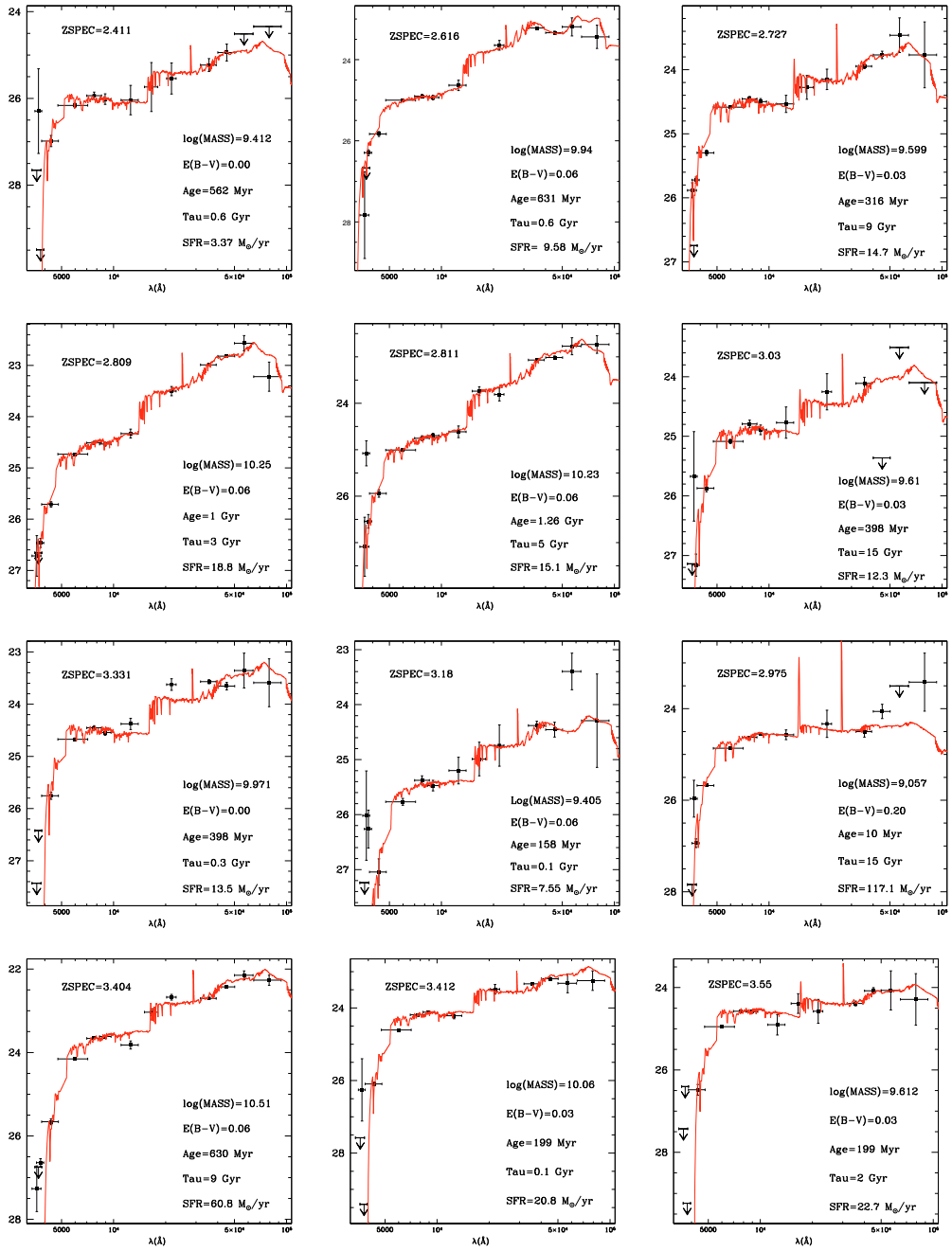

Fig. 2. Examples of the 14-bands SED-fitting for some of the galaxies in the order of increasing redshift from $z \sim 2.4$ (*upper left*) to $z \sim 3.5$ (*lower right*). In each panel we plot the photometry in the 14 bands (U to 8 μm) in black with relative errors and in red the best-fit solution. The two emission lines that are visible in many SEDs are the [OII] and Hα emission respectively, which are proportional to the SFR. The best-fit parameters for each galaxy and the spectroscopic redshift are also reported.

indicator. If we included it in the SED-fitting assuming a mean [OIII] flux as inferred in local star-burst galaxies corresponding to a ratio $f([\mathrm{OIII}])/f([\mathrm{OII}]) = 0.32$, the output of the fit did not change.

4. Physical properties: results

4.1. Total stellar masses, ages, dust extinction

We present here the main results for the stellar masses and ages of our sample. The values are those obtained with the CB09 models. For reference and comparison to previous work we also report the relative values obtained with the BC03 (in parenthesis). The total stellar masses that are found span a range 10^9–10^{11} $M_\odot$, with a median value of $5.3(7.5) \times 10^9$ $M_\odot$. These values are similar to those found by Shapley et al. 2003 (which were obtained with the even older BC96 models). The median age of our sample is 320 (500) Myr, very similar to the Shapley et al. value, while the $E(B-V)$ best-fit parameter is smaller 0.06(0.06) vs. 0.15. The discrepancies in the best-fit $E(B-V)$ arise in part from the different model of star formation history adopted in the SED-fitting (Shapley et al. use a constant star

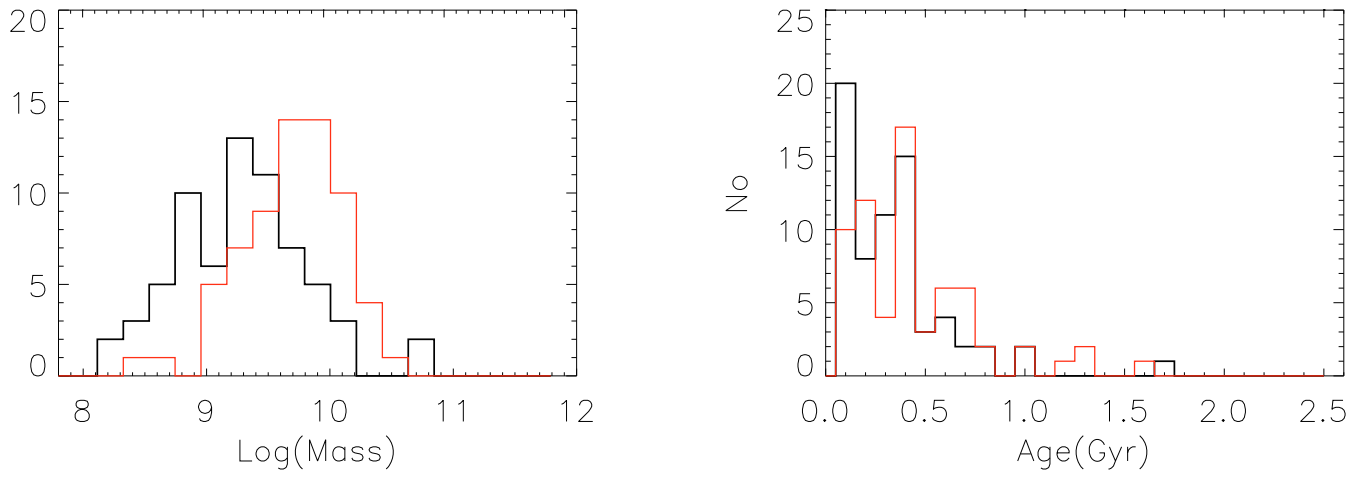

Fig. 3. *Left*: the distribution of stellar masses for LBG_L (black histogram) and LBG_N (red histogram). *Right*: the distribution of best-fit galaxy ages.

formation history) and in part from the slightly different color selection criteria adopted in this paper compared to previous works (see also end of this section).

Following the approach used in P07 we compared the properties of LBG_L to those of LBG_N. We found that the masses of LBG_N are larger than the masses of LBG_L and that the galaxies without an emission line are somewhat older. The median values with relative uncertainties are reported in Table 1 and the distributions are shown in Fig. 3. To assess the differences between the two samples in the physical parameters and their statistical significance, we performed a non-parametric Kolmogorov-Smirnov (K-S) test on the age and mass distributions. We found that the difference is indeed highly significant for the mass distribution ($P = 0.000$), while only weakly significant for the age distributions ($P = 0.136$).

The difference between the two samples at $z \sim 3$ is much less pronounced than at higher redshift: at $z \sim 4$ the masses of LBG_N were five times larger than the emitters, while in the present work the difference is only around a factor of 2. Similarly the difference was larger than a factor of 2 at higher z and now only around 25% for the ages, with very low significance. Moreover, at variance with the previous work, the age range spanned by LBG_L and LBG_N is basically equal.

In P09 we found that at redshift 3 to 6 there was a significant lack of massive galaxies with high EW amongst the LBG_L. In other words, although there was no clear correlation between EW and stellar mass, all galaxies with $EW_0 > 80$ Å (9 out of a sample of 70) had stellar masses equal or below the median mass. There are only three galaxies with $EW_0 > 80$ Å in the present sample, and their masses are indeed smaller than the median mass. Therefore the effect may be present, but is definitely much less pronounced than at higher redshift.

The $E(B-V)$ derived from the SED-fit are small, with a median value of 0.06 ± 0.012 and 0.03 ± 0.009 for LBG_N and LBG_L respectively. In accordance with previous results at higher redshift (P07) and with Shapley et al. (2003), we find that LBG_L tend to show less dust extinction: the difference between the sub-sample is small but significant (PKS = 0.012). To confirm this result, we also evaluated the continuum UV-slope from broad band V and I, data assuming that the continuum can be represented by a simple power law of the form $f_\lambda \propto \lambda^\beta$: the median values for the two sub-sample are $\beta = -1.15 \pm 0.11$ for LBG_N and -1.33 ± 0.12 for LBG_L. Again, this difference indicates that there is a diversity in dust extinction between the two sub-samples. We note that although the trend is similar to the one found by Shapley et al. (2003), they report slightly redder slopes for their LBGs for a given EW, ranging from –0.73 for the absorbers to -1.1 for the strongest emitters (but their beta values are evaluated from the $G-R$ colors, while our slopes are from V and I band data). On the other hand our values are similar to those reported by Hathi et al. (2008) for $z \sim 3$ LBGs, which is $\beta = -1.1 \pm 0.2$ and by Adelberger & Steidel (2000), which is $\beta = -1.5 \pm 0.4$.

We finally report a significant if very scattered correlation between the total stellar mass and the extinction, in the sense that the most massive galaxies tend to show more dust.

4.2. Star formation rates from ultraviolet continuum and SED-fitting

There are different ways of estimating the star formation rates (SFR) in LBGs. First the SFR can be estimated from the UV continuum luminosity using Kennicut (1998): $SFR_{UV} = 1.4 \times 10^{-28}\ L_\nu\ M_\odot\ \mathrm{yr}^{-1}$, where L_ν is the luminosity at rest-frame 1400 Å in units of erg s^{-1} hz^{-1}. This relation assumes a 10^8 year timescale for a galaxy to reach the full UV luminosity, so for the youngest objects the conversion could underestimate the true SFR. The UV emission is very sensitive to the presence of dust and can be attenuated even by small amounts: we corrected for this using the slope of the UV rest-frame continuum determined from the V and I band data and assuming a Calzetti law.

A second value is given by the SED-fit output SFR_{SED}. This clearly depends on the model assumed for the star formation history, in our case the exponentially declining star formation rate with e-folding time τ.

The median values for the two samples obtained for the SFRs in both ways are reported in Table 1. We found no significant differences between LBG_L and LBG_N, which agrees with P07 for $z \sim 4$ sources.

A commonly used measure to assess the importance of the current episode of star formation to the buildup of the stellar mass in galaxies is the specific star formation rate (SSFR) i.e. the star formation rate per unit mass. It is well known that more massive galaxies have lower SSFR (e.g. Erb et al. 2006) and that at a fixed stellar mass, the SSFR declines with increasing redshift (e.g. Reddy et al. 2006; Feulner et al. 2005). In Fig. 4 we

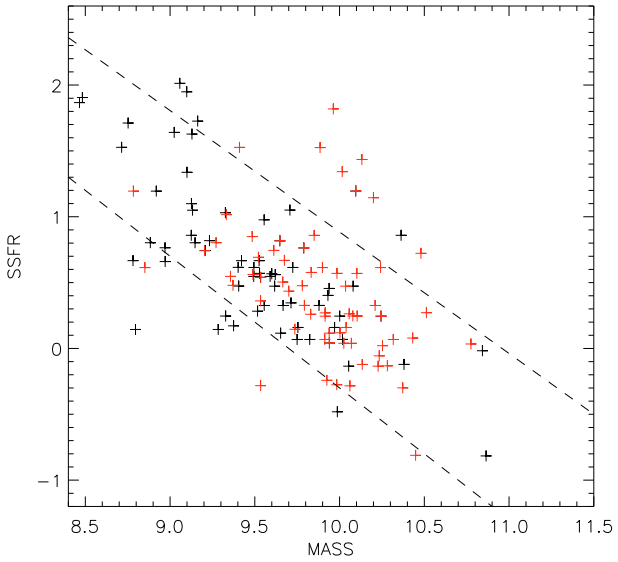

Fig. 4. Specific star-formation rate vs. stellar mass. The two dashed lines indicate constant values of SFR of 100 and 5 $M_{\odot}$ yr^{-1}. Red symbols are $LBG_{\rm N}$ and black ones are $LBG_{\rm L}$.

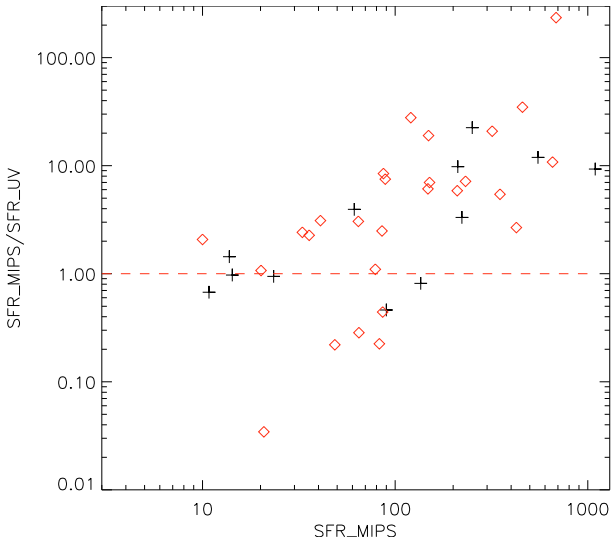

Fig. 5. Ratio of MIPS-derived SFR to SED-fitting values versus the MIPS-SFR. Red symbols are $LBG_{\rm N}$ and black symbols are $LBG_{\rm L}$. Although the rate of MIPS detection for $LBG_{\rm N}$ is twice that of $LBG_{\rm L}$, the two samples fall on the same relation.

plot the SSFR vs total stellar mass: the two quantities are anti-correlated with high probability (a Spearman' rank test gives a correlation coefficient of −0.6). In practice, galaxies with lower stellar mass are assembling a much higher fraction of their mass with the current star formation episode compared to more massive objects.

4.3. MIPS detection and infrared-determined star formation rates

At redshift ∼2.4 the mid-IR (5–8.5 μm) features associated with PAH emission, which are ubiquitous in local and $z \sim 1$ star-forming galaxies, are shifted into the MIPS 24 μm filter. We searched for counterparts of our LBGs in the GOODS-MUSIC 24 μm MIPS catalog (see Santini et al. 2009, for details). Note that galaxies with a mid-IR excess so that the MIPS flux is probably due to AGN activity rather than star formation (see also Fiore et al. 2008, for the proper definition) are flagged as AGNs in the revised version of the GOODS-MUSIC catalog we used and therefore were excluded from our initial sample selection (see also Sect. 2). Therefore we assume that the 24 μm flux is due to star formation.

We found a total of 39 objects with clear detections. Of these, 12 are $LBG_{\rm L}$ and 27 are $LBG_{\rm N}$, indicating that the detection rate of $LBG_{\rm N}$ is twice as high as that of the line emitters. As expected, the subset of MIPS-detected sources is on average brighter (in z–band) and at a slightly lower redshift than the entire sample. The MIPS-detected sources all belong to the most massive end of the stellar mass distribution, while other properties such as age and morphology (see later) are in the average range. In particular the mean log(Mass) of MIPS-detected galaxies is 0.48 dex higher than the rest of the sample, and this can explain the higher detection rate for $LBG_{\rm N}$.

Reddy et al. (2006) found similar results for optically selected (UGR) star-forming galaxies at $z \sim 2$: the age distributions of 24 μm detected and non-detected galaxies are similar, while the mass distributions are offset in a way that undetected galaxies have an average log(M) of 0.4 dex lower than for 24 μ detected galaxies. The MIPS-detected galaxies have a weaker Lyα emission and stronger interstellar absorption lines, which is consistent with our results.

Following the approach outlined in Santini et al. we derived the total IR luminosity and then the MIPS-inferred total SFR. As noted by Reddy et al. 2006, the conversion from the 24 μm flux to total IR luminosity and then to unobscured SFR are subject to many uncertainties. For our galaxies, accurate spectroscopic redshifts are known and this put us at the advantage of knowing exactly the location of the PAH features and their contribution to the 24 micron flux. Nevertheless we point out that there are still many sources of uncertainties in the conversion from 24 micron flux to total IR luminosity due to the modeling of the PAH features, which depend on the galaxy metallicity, galaxy environment, galaxy size, star formation history, and on the ionizing radiation field (Calzetti et al. 2007).

The derived $SFR_{\rm MIPS}$ are on average higher than both $SFR_{\rm SED}$ and $SFR_{\rm UV}$. We also found a clear trend that the $SFR_{\rm MIPS}/SFR_{\rm SED}$ tend to be ∼1 for objects with moderate star formation rates, while becoming $\gg$1 for objects with high SFR, as shown in Fig. 5. Both $LBG_{\rm L}$ and $LBG_{\rm N}$ seem to follow this trend. One possible explanation is that in objects showing $SFR_{\rm MIPS} \gg SFR_{\rm SED}$, the MIPS emission is not (entirely) due to star formation, but may be still partially due to AGN contribution, even after the exclusion of the clearly obscured AGNs. However, since the trend extends also to values lower than unity and is present at all redshifts (see Santini et al. 2009), it is possible that it reflects a change in some intrinsic physical property of star-forming galaxies, like metallicity. Galaxies with sub-solar metallicities have lower mid-IR emission (at least at 8 μm, Calzetti et al. 2007) and higher UV luminosity than solar ones for a given level of SFR. The observed trend could therefore be related to a metallicity trend. Unfortunately, a direct check of this is not feasible. Reliable metallicities cannot be inferred from broad-band SED-fitting, and high resolution spectroscopy is necessary to properly distinguish between SEDs characterized by different lines and hence metallicities.

Finally the observed trend could also be due to a failure of the assumed modeling of star formation history for example in galaxies with very high star formation.

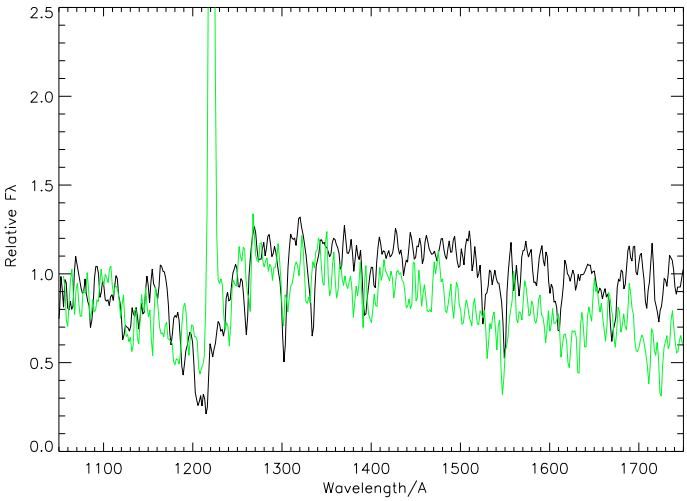

Fig. 6. Stacked spectra of LBG_N (black line)and LBG_L (green line). Besides the obvious difference in the Lyα region, the different spectral slope and strength of the absorption lines are also clearly shown.

5. Spectral properties

The majority of the spectra were retrieved from the GOODS VIMOS database. Because relatively few spectra and redshifts were obtained from the other programs, we decided to make a composite spectrum using only the VIMOS data. The homogeneity of the data set in terms of resolution, depth, and calibration accuracy made it easier to add up the spectra, even if the number of sources was reduced.

The 1-D spectra are distributed in fits format from the GOODS database[1]: they are calibrated both in flux and wavelength. For details on reduction and calibration see Popesso et al. (2009). The final redshift uncertainty quoted there is $\sigma_z = 0.0013$, obtained from a comparison between redshifts of the same objects obtained more than once with different set-ups.

The spectra were brought to rest-frame and co-addition was performed adopting a sigma–clipping procedure to eliminate sky-subtraction residuals, zero-count pixels due to CCD gaps, and other spectral blemishes. After several tests, the best results were obtained when a single 3σ clipping iteration was adopted. On average more than 90% of all galaxies in a given bin contributed to the stacked spectrum at any given wavelength.

In Fig. 6 we present the composite spectrum of all LBG_L and compare it to the LBG_N spectrum after normalizing the two spectra at 1280 Å. Besides the obvious difference of the presence of bright Lyα in the spectrum of LBG_L, we note that the spectrum of LBG_N is flatter than the spectrum of LBG_L, which agrees with the higher value of $E(B-V)$ derived from the SED-fit and indicating in LBG_N more dust than in the LBG_L. Furthermore, in the LBG_N spectrum the interstellar absorption lines are more prominent than in the LBG_L spectrum: this is more evident for the low ionization lines (SII1260, OI+SiII1303, CII1334, SiII1536), while for the high ionization lines the difference is not as marked. This was already observed in more detail by Shapley et al. (2003), who found that the kinematic offset between the Lyα line and the interstellar absorption lines also depends on the Lyα emission strength. A detailed analysis of the spectral stacks like in Shapley et al. is not allowed by the S/N of our composite spectra. Our aim here was only to check the resulting spectral stacks for consistency with previous work.

[1] http://www.eso.org/science/goods/spectroscopy/vimos.html

6. X-ray emission

The field was observed by Chandra in the 2 Ms exposure (Luo et al. 2008). We therefore searched for signatures of X-ray emission from our sample of LBG_L and LBG_N.

We remind that in the initial sample selection we excluded spectroscopically confirmed broad line and narrow line AGNs (BLAGNs and NLAGNs respectively). The first (BLAGNs) were easily spotted since they usually show a broad Lyα line, with typical FWHM of several thousands km s^{-1}, clearly resolved even in our low resolution spectra. The NLAGNs were recognized by the presence of high excitation emission lines in the spectra like NIV, CIV, HeII. Clearly in this case there could be more ambiguity, since these lines depend also on the S/N of the spectra, on the relative line ratio and on the spectral range observed. Therefore we cannot exclude that some NLAGNs could still be included in our sample.

Assuming that we removed all AGNs, we searched for possible X-ray flux associated to the LBGs, as due to star-burst emission. We cross-correlated our catalog with the 2 Ms Chandra point source list by Luo et al. (2008). The survey covers an area of 436 arcmin^2 and reaches on-axis sensitivity limits of 1.9×10^{-17} and 1.3×10^{-16} erg s^{-1} cm^{-2} for the 0.5−2.0 and 2−8 keV bands, respectively. Two objects (both classified as LBG_L) are present in the Chandra 2 Ms catalog as individual detections: # 11006 and # 8543. They were observed spectroscopically by Mainieri et al. (2006, who list them as LEX (emission line galaxies). However, from soft band fluxes (5.37 and 3.7×10^{-16} erg s^{-1} cm^{-2} respectively) and optical magnitude we derived ratios of X-ray to optical flux that fall within the region populated by AGNs (e.g. Hornschemeier et al. 2001).

The detection rate is comparable to Lemher et al. (2005), who found seven individually detected objects out of 449 U-dropouts, while Laird et al. (2006) presented a higher detection rate in the HDF-N area: in their spectroscopic sample of 89 LBGs they found X-ray emission from four galaxies, or 4.5%.

We stacked the X-ray undetected sources following the procedure adopted by Laird et al. (2006). The final stacked image corresponds to a total integration time of 0.26 Gs. As background we used the images produces by Luo et al., which are available at the Chandra survey web site. The flux at each source position was summed using a box cell of 6×6 pixels, corresponding to approximately 3″ a side. This value was chosen following Laird et al., who determined that a radius of ∼1.5″ maximizes the signal to noise in stacked detection of U-dropouts. The total counts were summed and the background was determined in an area of the same aperture. The result is a detection with $S/N = 4.1$ in the soft band (0.5−2 Kev), and a non-detection in the hard and total bands. The total net source counts in the soft band was 76 for 128 sources, implying a mean source count of 0.59. This is basically equal to the result of Laird et al., who reported an average 0.58 net counts for their sample of 277 HDF-N U-dropouts in the 2 Ms observations, while Lemher et al. found an average 0.44 counts per source. Assuming the stacked X-ray flux is due to star formation activity, we determined the average unobscured SFR implied by the X-ray. The flux corresponding to the average count rate is 2.3×10^{-18} erg s^{-1} cm^{-2}. At the mean redshift of the sample ($z = 2.85$) this corresponds to a luminosity in the 2–8 Kev rest-frame band of 1.62×10^{41} erg s^{-1}. We applied the conversion from X-ray flux to the SFR derived by Nandra et al. (2002), assuming a Salpeter IMF (as in our models). We derived an average unobscured $SFR_X = 29.1\ M_\odot$ yr^{-1}, slightly higher than both SFR_{UV} and SFR_{fit}.

Most importantly, in the context of the present work, when we stacked the fluxes of the LBG_L and LBG_N separately we did not find any significant difference. In particular, we found a total S/N of 2.1 for the LBG_L and $S/N = 2.6$ for the LBG_N. Again, we run a nonparametric K-S test on the individual counts for each group and found that the two distributions are perfectly compatible with each other ($P = 0.99$). We further probed this by stacking only the strongest emitters with an observed Lyα $EW > 100$ Å and obtained a similar result. Therefore we conclude that the X-ray properties do not depend on the presence and strength of the Lyα emission line or, at most, are only weakly correlated.

Table 2. Average morphological properties of LBG_L and LBG_N.

Property	LBG_L	LBG_N	$P(K-S)$
N_{gal}	66	66	
Concentration	2.55	2.57	0.52
Gini	0.47	0.46	0.54
Asymmetry	0.11	0.097	0.291
M_{20}	–1.40	–1.41	0.989
Ellipticity	0.258	0.323	0.203
Size	3.89	4.62	0.056
Area	154	207	0.020
Clumpy obj.	19/66	19/66	–

7. Morphological properties

Even for the lowest redshift objects in the sample, the ACS z-band samples the rest UV-emission (~3000 Å or shorter). The UV morphology tends to be patchy and irregular even for local galaxies (e.g. Gordon et al. 2004). However, high redshift galaxies have irregular morphologies not only in the UV, but also at longer rest-frame wavelengths (Papovich et al. 2005; Dickinson et al. 2005), indicating that the light is always dominated by the young stellar component. The most popular explanation is that these irregular systems represent mergers (e.g., Conselice et al. 2003). Alternatively it could be that the different components observed are just clumps of star formation rather than different merging systems. It is therefore interesting to determine if the morphology is connected to the other physical and spectral properties of the galaxies.

We analyzed the high resolution ACS z-band morphologies of our galaxies. In Fig. 8 we show the thumbnails of some of the galaxies in our sample in order of increasing redshift. We performed a non parametric analysis as in Scarlata et al. (2007). The program initially determines the Petrosian radius and then uses it as semi-major axis of an elliptical aperture where it calculates the following parameters: asymmetry, concentration, Gini coefficient, and second-order moment of the brightest 20% of galaxy pixels. The Gini coefficient (G) describes how uniformly the flux is distributed among galaxy pixels. The Gini statistic assumes values from 0 (if the galaxy light is homogeneously distributed among galaxy pixels) up to 1 (if all the light is concentrated in 1 pixel, regardless of its position in the galaxy) The concentration $C = 5\log(r80/r20)$ with $r80$ and $r20$ the radii including 80% and 20% of the total galaxy light, respectively, quantify the central density of the galaxy light distribution. M_{20} is the second-order moment of the brightest 20% of the galaxy flux (Lotz et al. 2004). For centrally concentrated objects, M_{20} correlates with the concentration C; however, M_{20} is also sensitive to bright off-centered knots of light. The asymmetry (A) quantifies the degree of rotational symmetry of the light distribution. A is measured by calculating the normalized difference between the galaxy image and the image rotated by 180 deg. A correction for background noise is also applied (as in Lotz et al. 2004). Finally we also used the ellipticity (ϵ) of the light distribution, as measured by SExtractor (Bertin & Arnouts 1996).

As shown in Scarlata et al. (2007), this non-parametric method is very efficient in quantifying galaxy morphology. The quantities above provide complementary, but also redundant, information on the galaxy structure. For a complete description and also the uncertainties on the parameters see Scarlata et al. (2007). We only remark here that using the Petrosian radius we were not affected by distance because surface brightness dimming does not change the shape of a galaxy light profile and therefore it does not affect the Petrosian index. For this reason we could compare the morphology of objects even if our sample spans a relatively large redshift range. We are aware that our method to calculate the Gini coefficient (inside a Petrosian aperture) may introduce some compression in its dynamic range and somewhat limit its distinguishing power (as argued by Law et al. 2007). In addition to the above parameters, we visually inspected the individual z-band thumbnails to check for multiple peaks of emission: clearly this is a more subjective and less precise analysis. Separate median values for LBG_L and LBG_N are reported in Table 2. In Fig. 7 we show the G, M_{20}, A, C and ϵ values for all galaxies analyzed, with separate symbols and colors for LBG_L and LBG_N.

We found that the $z \sim 3$ LBGs have median values $G \sim 0.48$, $M_{20} \sim -1.46$, $C \sim 2.6$ and $A \sim 0.12$. A comparison of the absolute values to those derived by other studies is not meaningful, because they depend on the S/N ratio and on the choice of aperture within which they are measured (Lisker 2008). However, our aim is a relative comparison between LBG_N and LBG_L: this is possible because the possible systematic errors are similar for both populations.

As for the physical parameters, a series of Kolmogorov-Smirnov tests was performed to assess the probability that in each case the LBG_L and LBG_N are drawn from different distributions for all the five parameters (A, G, C, M_{20} and ϵ), plus area and size. The probability P for each test is also reported in Table 2. In almost all cases (with the exception of size and area) there were no substantial differences in the morphology of galaxies. The morphological analysis was also repeated restricting the two sub-samples, LBG_N and LBG_L, to galaxies brighter than $z_{850} < 25$, and the results did not change.

This is at variance with what was suggested by Vanzella et al. (2009), who found a higher concentration for $z \sim 4-5$ galaxies with Lyα emission. Note however that their sample is smaller and the claimed difference has less than 2σ significance. Like Vanzella et al., we also found that galaxy size and area depend on line emission properties: but this could be a consequence of the lack of bright (massive) galaxies with large EW, rather than a real dependence on line emission. If we plot the size vs. EW of our galaxies (analogous to Fig. 19 of Vanzella et al.), we found that galaxies with small or negative EW span the whole range of sizes, while large EW objects tend to be very small. This same trend was found by Law et al. (2007) in an analysis of combined u, v, i and z band data on LBGs at $z \sim 3$. They also found a possible correlation between Lyα and the Gini parameter, but they noted that the correlation is not well defined.

In conclusion we did not find much evidence for a strong morphological dependence of the emission line properties, but we found that line emitters tend to be small galaxies, while there are both small and large galaxies among LBG_N.

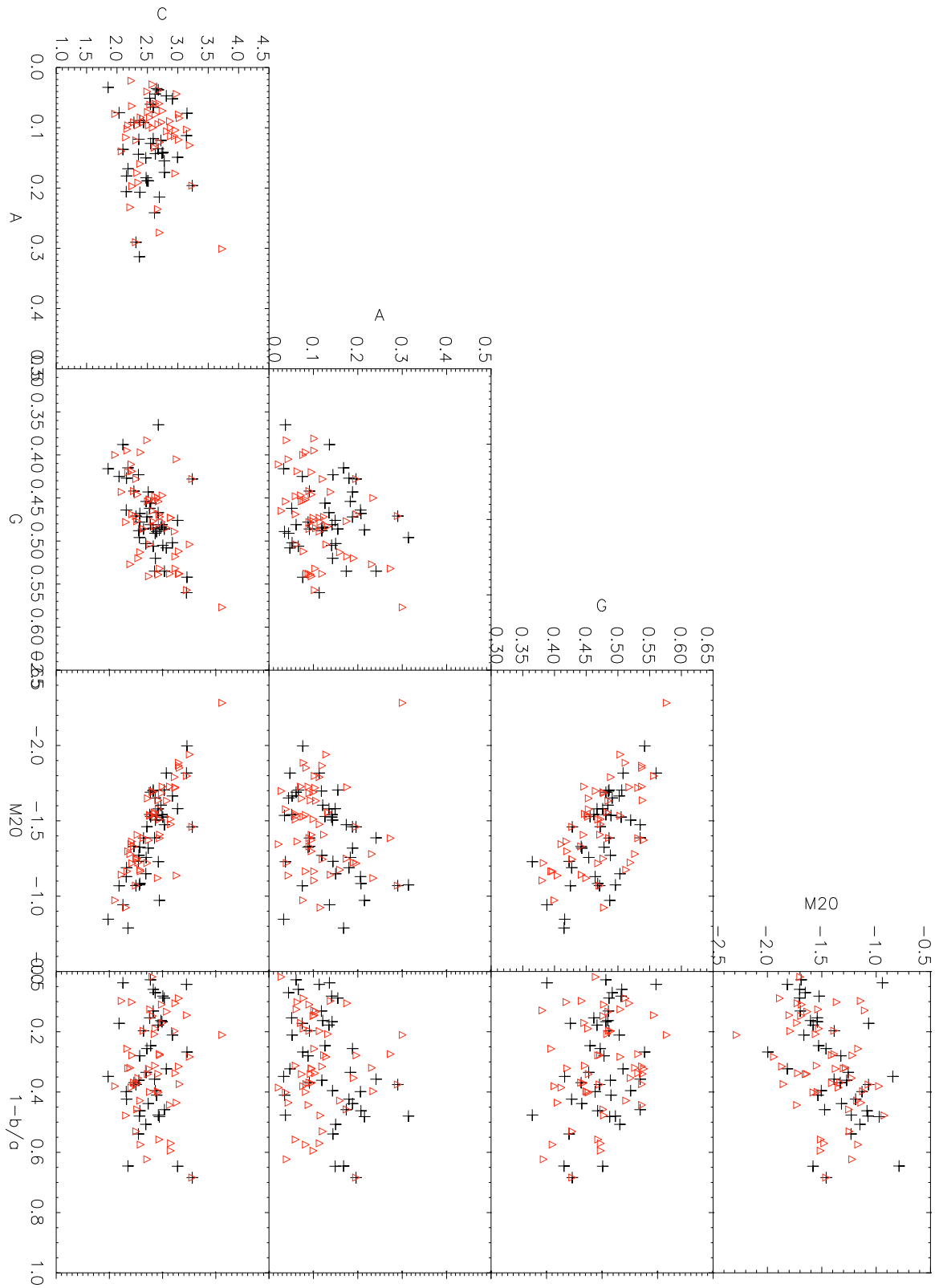

Fig. 7. Relations between the nonparametric diagnostics (M_{20}, G, A, C, and $\epsilon = 1 - b/a$). The main correlations among some of the parameters, like M_{20}, C, and G, are clearly visible in these diagrams. In each panel black + are $LBG_{\rm L}$ and red triangles are $LBG_{\rm N}$.

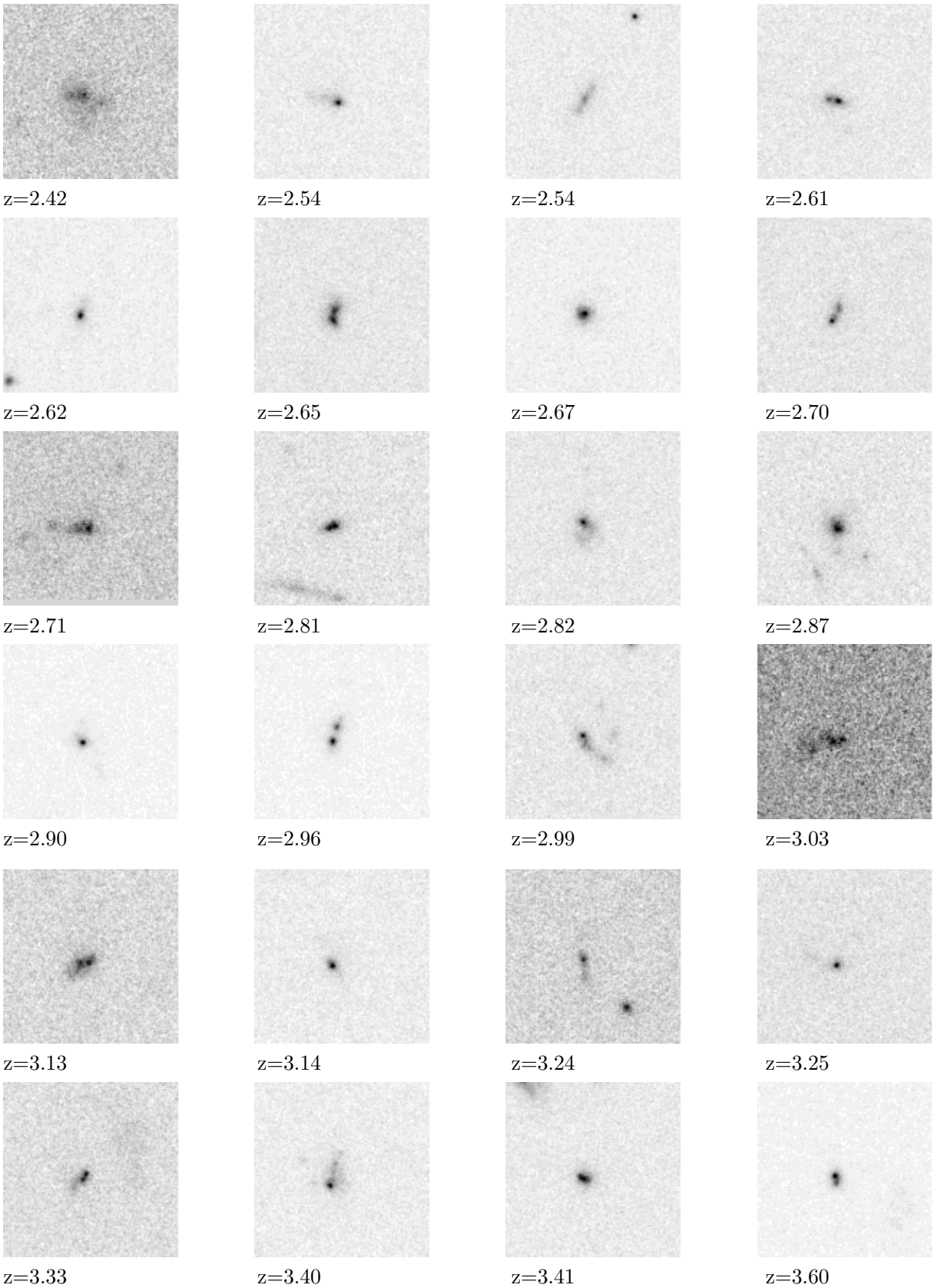

Fig. 8. Thumbnails of some of our LBGs, in order of increasing redshift. Each image is taken in the z-band and is $4'' \times 4''$ in size.

8. Summary and discussion

We briefly summarize the main results of this work and then attempt to interpret them in the context of a simple scenario.

1. At $z \sim 3$ $LBG_{\rm N}$ are significantly more massive than $LBG_{\rm L}$.
2. The ages of $LBG_{\rm L}$ and $LBG_{\rm N}$ are comparable. The median age of $LBG_{\rm N}$ is somewhat larger than the median age of $LBG_{\rm L}$, but at less than 3σ level.

3. The current SFR (SFR_{UV} or SFR_{SED} is similar for both groups, as expected given the initial selection. This is further confirmed by the stacked X-ray flux, related to unobscured star formation: no relevant differences are observed between the two groups.
4. Given that ages and SFR are similar for both LBG_N and LBG_L the larger average masses of LBG_N imply that these galaxies had higher star formation in the past. We remind that SFR_{UV} is sensitive only to current star formation rate on timescales of less than 100 Myr, while many galaxies have ages higher than this.
5. The SSFR is a strong function of mass and is higher for low mass objects and therefore tends to be higher for LBG_L.
6. The MIPS detection rate of LBG_N is 2.5 times higher than for LBG_L.
7. All LBGs have small dust extinction as expected: LBG_N have relatively higher dust content, as inferred by the higher $E(B-V)$ values derived from the SED-fitting and by the steepness of the stacked spectra.
8. We find no notable differences in the morphological parameters, with the exception of the smaller sizes and areas of LBG_L compared to LBG_N.

8.1. A simple scenario

The continuity and almost substantial overlap of physical and morphological properties of LBGs as well as the few trends we found substantially agree with the unification scheme between LBGs and LAEs proposed by Verhamme et al. (2008). In their model, almost all LBGs have intrinsically high Lyα emission ($EW \sim 60-80$ Å or larger), and the observed variety of Lyα strengths and profiles and ultimately the fact that these galaxies are selected as LBGs or LAEs is due to variations in the content of dust and HI (see also Atek et al. 2009). The assumed geometry is that of an expanding, spherical, homogeneous, and isothermal shell of neutral hydrogen surrounding a central star-burst emitting a UV continuum plus Lyα recombination line radiation from its associated H II region: dust is uniformly mixed to the HI gas and the variation of these two quantities shape the profile of the Lyα. Ultimately the main parameter responsible for these variations may be the galaxy mass. Indeed, if the most massive galaxies also contain more dust, as we observed given the correlation between $E(B-V)$ and stellar mass (although with a large scatter), a natural consequence is that massive galaxies would show Lyα with smaller EW or Lyα in absorption. This would naturally produce the large mass segregation observed between LBG_L and LBG_N, which is one of the strongest results of the present work. It would also explain the lack of massive galaxies with bright Lyα emission observed here and already pointed out in P09, and similarly the lack of luminous galaxies with bright Lyα emission observed by other authors (e.g. Ando et al. 2007).

Furthermore, in the Verhamme et al. model, no age constrains are derived from the presence of Lyα up to $EW \sim 100$ Å, as such equivalent widths can be obtained, especially for a constant star formation history even taking into account various degrees of dust suppression. This is at variance with other models which put a strong limitation on the maximum age of Lyα emitting galaxies (e.g. Mao et al. 2007; Mori & Umemura 2006). Therefore our result that LBG_L and LBG_N have very similar ages and the fact that we do find Lyα emitting galaxies with ages exceeding several hundred Myrs also nicely agrees with the Verhamme et al. model. They actually predict that objects with very bright Lyα ($EW \gg 100$ Å) should all be extremely young (less than 10–40 Myr), but in our sample of LBG_L we did not have any of these large EW galaxies. Last but not least, the lack of significant morphological differences between LBG_L and LBG_N also agrees with this scenario.

Possible outliers in this unifying scheme would be objects that have Lyα absorptions but at the same time show no indications for dust extinction, basically LBG_N with $E(B-V) = 0$. Most of the LBG_N indeed have $E(B-V) \neq 0$, and only three of them seem to be dust-free galaxies with no Lyα in emission. Clearly the $E(B-V)$ we estimated is subject to errors, so it could still be that a little dust is present: alternatively in these cases the n_{HI} could be playing a major role in suppressing the Lyα emission and/or there could be variations in the dust/HI ratio. Indeed Steidel (2008) argued that the Lyα emission strength and apparent redshift is strongly affected by gas near the systematic velocity of the galaxy, which is often absent in lower-mass objects. Therefore low mass objects naturally tend to show brighter Lyα emission than high mass ones.

To further test the above scenario, one would need to establish a solid relation between the total stellar mass of a galaxy and the neutral hydrogen content. Also the exact dependence between the amount of dust and the stellar mass, and the variation of dust/gas ratio still need to be explored in detail. Last but not least, dust geometry and the way dust and emitting sources are mixed could also influence the observed Lyα appearance. Recently Scarlata et al. (2009) considered various possibilities for the geometry of dust around emitting sources and found that the uniform dust screen is not able to reproduce all the observations, while a clumpy dust distribution better fits the data with no need to invoke differential extinction of Lyα and continuum photons for most of the galaxies.

8.2. Redshift evolution?

Although the simple scenario described before seems to fit both the correlation found at $z \sim 3$, and the absence of trends in other properties, some modification may be needed to account for the evolution in some of these properties/trends with redshift. Indeed, there are strong indications that some of the correlation between Lyα strength and LBGs properties change considerably with cosmic epoch. First of all, as discussed in the introduction, the simple fraction of LBGs that are also LAEs and ultimately the EW distribution of Lyα in LBGs at the various cosmic epochs is still a subject of debate. Most authors claim that the distribution of Lyα strength found at $z = 3$ by Shapley et al. (2001) remains valid at all redshifts (e.g. P07, Stanway et al. 2007; Dow-Hygelund et al. 2007), although the $z \sim 6$ population has a tail of sources with high rest-frame equivalent widths (Stanway et al. 2007). Other authors claim instead that at very high redshift almost all LBGs become strong Lyα emitters (e.g. Shimasaku et al. 2006). Finally, at lower redshift, Reddy et al. (2008) noted that among UV selected star-forming galaxies, the redshift ~3 (LBG) population has a higher incidence of Lyα in emission than the redshift ~2 (the so called BX population).

In this work we found further indication of evolution for other properties: first of all we found no age segregation at $z \sim 3$, while at $z \sim 4$ we reported that LBG_L were considerably much younger than LBG_N (P07). The difference in total stellar mass was also much more pronounced at $z \sim 4$ (P07), compared to this study.

At $z \sim 3$ we also found no significant evidence for morphological differences between LBG_N and LBG_L, but at lower redshift Law et al. (2007), using a different set of morphological parameters, found possible although not well-defined trends.

On the other hand, at $z \sim 4$ Vanzella et al. (2009) reported a marked difference in the Gini and concentration indexes of the two groups, with the LBG_L being more concentrated than the rest of the galaxies. Similarly at $z \sim 6$ the tentative results of Dow-Hygelund et al. (2007) showed that sources with Lyα emission are smaller on average than the i-dropout population in general. However, at variance with this study, Taniguchi et al. (2009) recently claim that there is no difference in the morphological properties between the two populations, LAEs and LBGs at $z \sim 6$. These discrepant results indicate that disentangling the morphological properties of high z galaxies and comparing different samples at different redshift is still far from trivial. In a forthcoming work we plan to analize the morphologies of LBGs at various redshift in greater depth, using a unique set of parameters, so that a consistent comparison can be made between the various cosmic epochs.

In any case, the above results strongly suggest an evolution of some fundamental property of galaxies, be it the dust content (e.g. Nillson et al. 2009) or the Lyα escape fraction (e.g. Nagamine et al. 2008), which shape the appearance of star-forming galaxies: it is therefore essential that they are taken into account by the models.

References

Adelberger, K. L., & Steidel, C. C. 2000, ApJ, 544, 218
Atek, H., Kunth, D., Schaerer, D., et al. 2009, A&A, 506, L1
Bertin, E., & Arnouts, S. 1996, A&AS, 117, 393
Bruzual, G., & Charlot, S. 2003, MNRAS, 344, 1000
Calzetti, D., Kennicutt, R. C., Engelbracht, C. W., et al. 2007, ApJ, 666, 870
Conselice, C. J., Bershady, M. A., Dickinson, M., & Papovich, C. 2003, AJ, 126, 1183
Cowie, L. L., & Hu, E. M. 1998, AJ, 115, 1319
Dayal, P., Ferrara, A., & Gallerani, S. 2008, MNRAS, 389, 1683
de Santis, C., Grazian, A., Fontana, A., & Santini, P. 2007, New Astron., 12, 271
Dickinson, M., Stern, D., Giavalisco, M., et al. 2004, ApJ, 600, L99
Dijkstra, M., & Wyithe, J. S. B. 2007, MNRAS, 379, 1589
Dow-Hygelund, C. C., Holden, B. P., Bouwens, R. J., et al. 2007, ApJ, 660, 47
Drory, N., Bender, R., Feulner, G., et al. 2004, ApJ, 608, 742
Eminian, C., Kauffmann, G., Charlot, S., et al. 2008, MNRAS, 384, 930
Erb, D. K., Steidel, C. C., Shapley, A. E., et al. 2006, ApJ, 647, 128
Feulner, G., Gabasch, A., Salvato, M. et al. 2005, ApJ, 633, L9
Finkelstein, S. L., Rhoads, J. E., Malhotra, S., Pirzkal, N., & Wang, J. 2007, ApJ, 660, 1023
Fiore, F., Grazian, A., Santini, P., et al. 2008, ApJ, 672, 94
Fontana, A., Donnarumma, I., Vanzella, E., et al. 2003, ApJ, 594, L9
Fontana, A., Pozzetti, L., Donnarumma, I., et al. 2004, A&A, 424, 23
Fontana, A., Salimbeni, S., Grazian, A., et al. 2006 A&A, 459, 745
Gawiser, E. 2009, New Astron. Rev., 53, 50
Giavalisco, M., Dickinson, M., Ferguson, H. C., et al. 2004, ApJ, 600, L103
Grazian, A., Fontana, A., de Santis, C., et al. 2006, A&A, 449, 951
Grazian, A., Salimbeni, S., Pentericci, L., et al. 2007, A&A, 465, 393
Gordon, K. D., Pérez-González, P. G., Misselt, K. A., et al. 2004, ApJS, 154, 215
Hathi, N. P., Malhotra, S., & Rhoads, J. E. 2008, ApJ, 673, 686
Hornschemeier, A. E., Brandt, W. N., Garmire, G. P., et al. 2001, ApJ, 554, 742
Hu, E. M., Cowie, L. L., & McMahon, R. G. 1998, ApJ, 502, L99
Iye, M., Ota, K., Kashikawa, N., et al. 2006, Nature, 443, 186
Kennicutt, R. C., Jr. 1998, ARA&A, 36, 189
Kovač, K., Somerville, R. S., Rhoads, J. E., Malhotra, S., & Wang, J. 2007, ApJ, 668, 15
Kurk, J., Cimatti, A., Daddi, E., et al. 2009, The Messenger, 135, 40
Lai, K., Huang, J.-S., Fazio, G., et al. 2008, ApJ, 674, 70
Laird, E. S., Nandra, K., Hobbs, A., & Steidel, C. C. 2006, MNRAS, 373, 217
Lamareille, F., Brinchmann, J., Contini, T., et al. 2009, A&A, 495, 53
Laursen, P., Razoumov, A. O., & Sommer-Larsen, J. 2009, ApJ, 696, 853
Law, D. R., Steidel, C. C., Erb, D. K., et al. 2007, ApJ, 656, 1
Lehmer, B. D., Brandt, W. N., Alexander, D. M., et al. 2005, AJ, 129, 1
Lisker, T. 2008, ApJS, 179, 319
Lotz, J. M., Primack, J., & Madau, P. 2004, AJ, 128, 163
Luo, B., Bauer, F. E., Brandt, W. N., et al. 2008, ApJS, 179, 19
Mao, J., Lapi, A., Granato, G. L., de Zotti, G., & Danese, L. 2007, ApJ, 667, 655
Maraston, C. 2005, MNRAS, 362, 799
Maraston, C., Daddi, E., Renzini, A., et al. 2006, ApJ, 652, 85
Marchesini, D., van Dokkum, P. G., Förster Schreiber, N. M., et al. 2009, ApJ, 701, 1765
Marigo, P., & Girardi, L. 2007, A&A, 469, 239
Mainieri, V., Rosati, P., Tozzi, P., et al. 2005, A&A, 437, 805
Malhotra, S., Rhoads, J. E., Pirzkal, N., et al. 2005, ApJ, 626, 666
Mori, M., & Umemura, M. 2006, Nature, 440, 644
Nagamine, K., Ouchi, M., Springel, V., & Hernquist, L. 2008, [arXiv:0802.0228]
Nandra, K., Laird, E. S., Adelberger, K., et al. 2005, MNRAS, 356, 568
Nilsson, K. K., Møller, P., Möller, O., et al. 2007, A&A, 471, 71
Nilsson, K. K., Tapken, C., Møller, P., et al. 2009, A&A, 498, 13
Ota, K., Iye, M., Kashikawa, N., et al. 2008, ApJ, 677, 12
Ouchi, M., Shimasaku, K., Akiyama, M., et al. 2005, ApJ, 620, L1
Papovich, C., Dickinson, M., & Ferguson, H. C. 2001, ApJ, 559, 620
Papovich, C., Dickinson, M., Giavalisco, M., Conselice, C. J., & Ferguson, H. C. 2005, ApJ, 631, 101
Pentericci, L., Grazian, A., Fontana, A., et al. 2007, A&A, 471, 433
Pentericci, L., Grazian, A., Fontana, A., et al. 2009, A&A, 494, 553
Pirzkal, N., Xu, C., Malhotra, S., et al. 2004, ApJS, 154, 501
Popesso, P., Dickinson, M., Nonino, M., et al. 2009, A&A, 494, 443
Reddy, N. A., Steidel, C. C., Fadda, D., et al. 2006, ApJ, 644, 792
Rhoads, J. E., & Malhotra, S. 2001, ApJ, 563, L5
Salimbeni, S., Castellano, M., Pentericci, L., et al. 2009, A&A, 501, 865
Santini, P., Fontana, A., Grazian, A., et al. 2009, A&A, 504, 751
Scarlata, C., Carollo, C. M., Lilly, S., et al. 2007, ApJS, 172, 406
Scarlata, C., Colbert, J., Teplitz, H. I., et al. 2009, ApJ, 704, L98
Shapley, A. E., Steidel, C. C., Adelberger, K. L., et al. 2001, ApJ, 562, 95
Shapley, A. E., Steidel, C. C., Pettini, M., & Adelberger, K. L. 2003, ApJ, 588, 65
Shimasaku, K., Kashikawa, N., Doi, M., et al. 2006, PASJ, 58, 313
Stanway, E. R., Bunker, A. J., Glazebrook, K., et al. 2007, MNRAS, 376, 727
Steidel, C. C., Giavalisco, M., Pettini, M., Dickinson, M., & Adelberger, K. L. 1996, ApJ, 462, L17
Steidel, C. C., Adelberger, K. L., Shapley, A. E., et al. 2003, ApJ, 592, 728
Steidel, C. C., 2008, Proceedings of the XXIVth IAP Conf., Far Away: Light in the young Universe, Paris
Straughn, A. N., Meurer, G. R., Pirzkal, N., et al. 2008, AJ, 135, 1624
Taniguchi, Y., Murayama, T., Scoville, N. Z., et al. 2009, ApJ, 701, 915
Vanzella, E.,Cristiani, S., Dickinson, M., et al. 2006, A&A, 454, 423
Vanzella, E., Cristiani, S., Dickinson, M., et al. 2008, A&A, 478, 83
Vanzella, E., Giavalisco, M., Dickinson, M., et al. 2009, ApJ, 695, 1163
Venemans, B. P., Röttgering, H. J. A., Miley, G. K., et al. 2007, A&A, 461, 823
Verhamme, A., Schaerer, D., Atek, H., & Tapken, C. 2008, A&A, 491, 89